doi:10.1038/nature11840

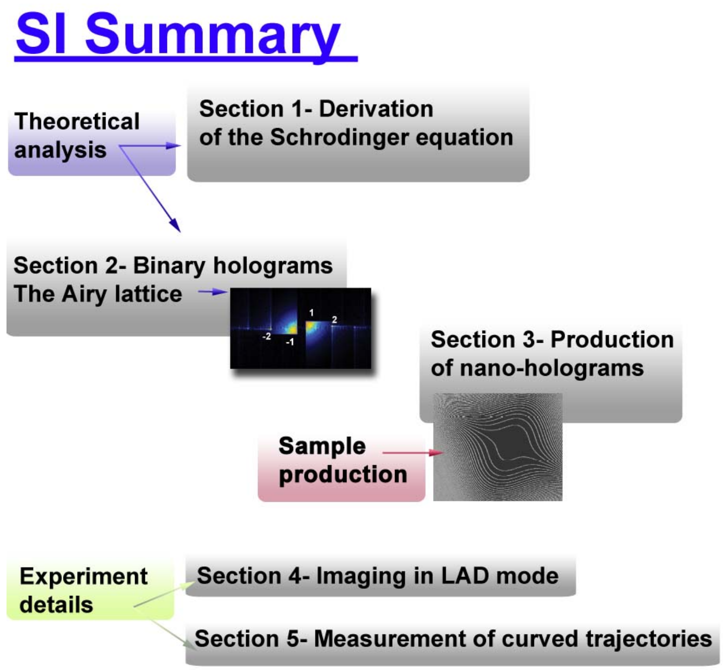

Section 1. Provides an analytical derivation of the Schrödinger equation or the Helmholtz equation from the Klein-Gordon equation for electrons. Section 2 provides a mathematical and numerical analysis of the diffraction patterns from binary nano-scale holograms designed with arbitrary phase. It also provides an extended derivation of the quadratic coefficient of each diffraction order of the Airy lattice. Using these quadratic coefficients, the parabolic trajectories of the diffracted orders can be deduced. Section 3 elaborates about the fabrication technique of the nano-holograms and gives a precise method for manufacturing them with an optimal resolution (that was needed in this experiment). Section 4 describes in details the experimental imaging technique (LAD mode) which allowed high magnification of the electron wave packet in the back focal plane. Section 5 elaborates about the method of measuring parabolic trajectories of Airy diffraction orders, and about the comparison made to the diffraction from a reference Bragg grating.

1 Quasi-relativistic Schrödinger equation– Ignoring spin effects, we may use the Klein-Gordon equation instead of the Dirac equation in order to find the wave function of a relativistic electron. For free space propagation (without any external potential):

$$-\hbar^2\frac{\partial^2}{\partial t^2}\Phi = (mc^2)^2\Phi - c^2\hbar^2\nabla^2\Phi. \tag{1}$$

The electron wavefunction plane wave solution is:

$$\Phi(r,t) = \Phi_0\exp(i\underline{p}\cdot\underline{r}/\hbar - iEt/\hbar), \tag{2}$$

where E, p satisfy the dispersion relation $E = \sqrt{c^2p^2 - (mc^2)^2}$. Classically, $E = \gamma mc^2$, $P = \gamma\beta mc$, $\gamma = 1/\sqrt{1-\beta^2}$ and $\beta = v/c$.
For small angle diffraction $p_\perp \ll p$ (paraxial approximation) we can derive a wave solution in the form:

$$\Phi(r,t) = \Psi(r_\perp, z)\cdot\exp(iPz/\hbar - iEt/\hbar), \tag{3}$$

Assuming slowly varying envelope and neglecting the second derivative of z, from Eq. 1 we obtain:

$$\left(\nabla_\perp^2 + 2ik_B\frac{\partial}{\partial z}\right)\Psi = 0, \tag{4}$$

where $\nabla_\perp^2 = \partial/x^2 + \partial/y^2$ is the transverse derivative and $k_B = p/\hbar = \gamma mv/\hbar = 2\pi/\lambda_B$ is the de-Broglie wave number of the electron. This equation has the same form as the paraxial Helmholtz equation, which describes the propagation of light beams in space (used to find the solution for Airy optical beams[2]), except that it includes the de-Broglie wave number.

Setting $z = \beta ct$ results in:

$$\left(\frac{\hbar^2}{2\gamma m_e}\nabla_\perp^2 + i\hbar\frac{\partial}{\partial t}\right)\Psi = 0, \tag{5}$$

which is the same as the Schrödinger equation that was solved (in 1D) by Berry and Balzas[1], with a relativistic correction to the electron rest mass.

2 The Airy lattice– The Airy lattice is a periodic lattice imposed with a cubic phase. A general formula that represents a lattice imposed with an arbitrary phase is (binary structure) [7]:

$$h(x,y) = \frac{1}{2}h_0(\mathrm{sgn}\{\cos[2\pi x/\Lambda + \phi(x,y)] + D_{cycle}\} + 1). \tag{6}$$

When electrons (or light) diffracts from the aforementioned binary structure, it decomposes to different orders; the complex amplitude of the m-th order diffracted beam is $\propto \exp(i\cdot m\phi(x,y))$. Any arbitrary phase can be imposed on this lattice. As an example a fork shaped structure[3,4] is generated by: $\phi(x,y) = l_c\tan^{-1}(y/x)$, where l_c is the topological charge. The diffraction pattern from this grating is a series of vortices. Each vortex has a different orbital angular momentum, which equals to $m\cdot l_c$. The radius of each vortex increases as a function of orbital angular momentum, thus, the diffraction from a fork shaped structure generates a series of vortices with different radii[3,4] and different orbital angular momentum as seen in Fig. 1 c .

However, when the hologram is imposed with the following cubic phase: $\phi(x,y) = c_xx^3 + c_yy^3$, we obtain the Airy lattice. In the case of Airy lattice, each diffracted order is imposed with a different cubic phase: $\propto \exp(i\cdot m(c_xx^3 + c_yy^3))$. In this case each Airy order propagates in a different quadratic trajectory. This is easily viewed in Fig. 1 a as each diffraction Airy order reach a different height (there is only a quadratic component in y axis).

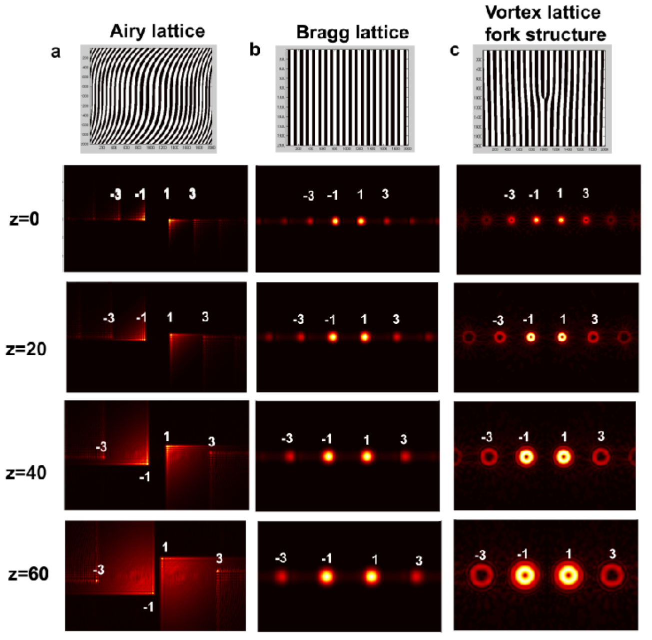

Figure 1 | **Comparison between the diffraction pattern from an Airy Lattice to fork shaped and Bragg lattice and their evolution in space. a,** Airy lattice. **b,** Bragg lattice. **c,** Vortex lattice. **a,** Different diffraction orders of Airy lattice have different quadratic coefficients proportional to 1/m. This is indicated as each order is elevated to a different height in y. The orders converge in x, while at the same distance Bragg orders diverge. **c,** The diffraction from a fork shaped structure generates a series of vortices with different radii.

Fourier transform of a cubic phase results in an Airy function:

$$Ai(x) = \frac{1}{2\pi}\int_{-\infty}^{\infty} e^{ipx}e^{i\frac{P^3}{3}}dp \tag{7}$$

The argument of the Airy function can be normalized by x_0:

$$Ai(\frac{x}{x_0}) = \frac{1}{2\pi}\int_{-\infty}^{\infty} e^{ip'\frac{x}{x_0}}e^{i\frac{(p')^3}{3}}dp' = \frac{1}{2\pi}\int_{-\infty}^{\infty} e^{ipx_0\frac{x}{x_0}}e^{i\frac{(x_0p)^3}{3}}dpx_0 \tag{8}$$

The quadratic component is proportional to $1/x_0^3$. However, in the case of Airy lattice, each order is diffracted with a different phase $\phi_m(p) = m\cdot(x_0p)^3$. Thus,

$$Ai_m(\frac{x}{x_{0m}}) = \frac{1}{2\pi}\int_{-\infty}^{\infty} e^{ipx_{0m}\frac{x}{x_{0m}}}e^{i\frac{(x_{0m}p)^3}{3}}dpx_{0m} = \frac{1}{2\pi}\int_{-\infty}^{\infty} e^{ipx_{0m}\frac{x}{x_{0m}}}e^{im\cdot\frac{(x_0p)^3}{3}}dpx_{0m} \tag{9}$$

The latter equation results in: $x_{0m} = x_0\sqrt[3]{m}$. This scaling factor is also demonstrated by a 1D Airy lattice (with an Airy modulation only in y) in Fig. 2. As seen, the 10-th minimum indicated by the white arrow is increasing as a function of order. The ratio between x_{0m} of different Airy orders was calculated numerically and fits the theoretical value: $x_{02}/x_{01} = 1.27 \approx \sqrt[3]{2/1}$, $x_{03}/x_{02} = 1.14 \approx \sqrt[3]{3/2}$ etc. The quadratic coefficient of each order is proportional to $\propto 1/x_{0m}^3 = 1/(mx_0^3)$.

Up to date, the trajectory measurement was carried out by capturing several profile pictures in several planes following the Fourier plane. However in the case of Airy lattice, the quadratic component can be indicated in a single plane (after Fourier plane). The deflection in y axis of each order is $y(m) = 1/m * z^2/4k_B^2 y_0^3$, so the deflection in y of each order is proportional to 1/m.

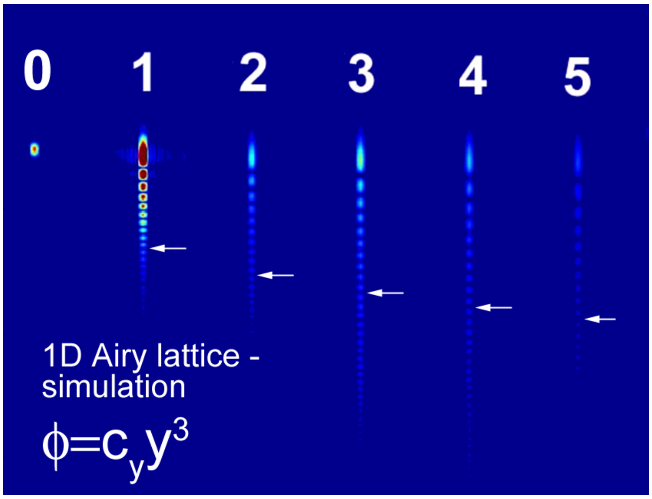

Figure 2 | **Airy 1D lattice**. Each order is imposed with a different cubic phase, thus, at the Fourier plane it has a different scaling factor $y_{0m} = y_0 \sqrt[3]{m}$. The different scaling factor of each order is indicated by the white arrow.

The Airy lattice is a novel type of lattice. Although it decomposes to different orders which diffract to different directions, each order stays localized (unlike Bragg lattice) and anomalously propagate along a curved trajectory.

3 Nanoscale hologram preparation

– Our hologram design method was to construct a binary diffraction grating with the following shape[6,7]:

$$h(x,y) = \frac{1}{2} h_0(\mathrm{sgn}\{\cos[2\pi x/\Lambda + c_x x^3 + c_y y^3] + D_{cycle}\} + 1). \tag{10}$$

In this way, a cubic phase is imposed on a carrier frequency. The carrier period is Λ, h_0 is the ridge height of the binary phase mask. D_{cycle} is an arbitrary duty cycle factor. Setting the duty cycle factor $0 < D_{cycle} < 1$ to high values (0.8 , 0.9...), gives a hologram with very narrow stripes (almost lines). This method was chosen because it allows us to use the highest resolution writing mode of the focused ion beam (FIB) (with lines). The nanoscale holograms see Fig. 3 were prepared by sputter depositing 10 nm Au layer onto a 50 nm silicon membrane chip, then milling the desired pattern with a Raith IonLine focused ion beam machine. The machine mills with a 35 keV Ga ions beam, and we used 2.6 pA ion beam current with step size of 2nm and dwell time of 1.54 msec. This gives an effective dose of 20000 pC/cm for single-pixel-line milling. These conditions milled through the entire gold layer and in addition about 20 nm of the silicon nitride membrane. The milling was done over areas of 30 μm X 30 μm. This method enabled us to achieve high resolution writing, without breaking the membrane chip. This kind of resolution was necessary for our experiment.
The parameters of the fabricated nano-holograms are:

1. A 2D Airy lattice structure with carrier (AWC): $\Lambda = 400$ nm and $a_{x,y} = 2 \cdot 10^{10} \cdot 2\pi/(400 \cdot 10^{-9})$ $[1/\mathrm{m}^3]$ shown in Fig. 1b.
2. A 2D structure with no carrier (ANC): $a_{x,y} = 2 \cdot 10^{10} \cdot 2\pi/(400 \cdot 10^{-9})$ with the same quadratic component as AWC $[1/\mathrm{m}^3]$ as shown in Fig. 1c.
3. A 1D structure with carrier: $\Lambda_X = 400$ nm, and quadratic trajectory only in y: $a_y = 2 \cdot 10^{10} \cdot 2\pi/(400 \cdot 10^{-9})$ $[1/\mathrm{m}^3]$.
4. A simple periodic Bragg lattice (BR) structure with a period $\Lambda_X = 100$ nm. It served as a reference scale for the measurement.

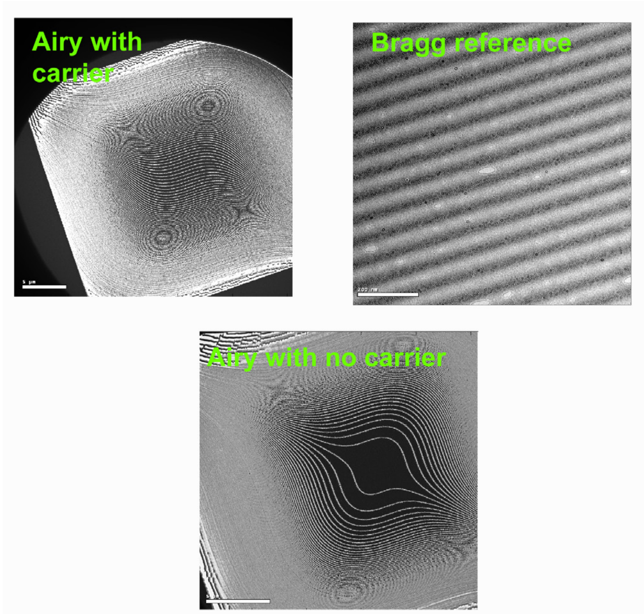

Figure 3 | **Micrograph of AWC, ANC BR.** The aforementioned method of writing enabled us to achieve high resolution, without breaking the membrane chip. This kind of resolution was necessary for our experiment.

4 Experiment details

– We used a Tecnai F20@ FEG-TEM and studied the generation and evolution of electron Airy beams by varying the focal lengths of the TEM magnetic lenses[4]. We imaged the electron wave packet as it evolved in different planes between the back focal plane and the image plane. The profiles were taken in FEG-TEM low angle diffraction mode (LAD), for which the objective lens is with low current (around 7 % of the maximal current). This enabled high magnification of the back focal plane. Setting a high current in the magnetic condenser lens and using an area adjuster, gave a relatively low convergence electron beam. Then, by a 'Free Lens Control' software increasing the current in the diffraction magnetic lens only (which was the only lens we changed during the measurements), we imaged different planes following the back focal plane. A Gatan camera model 694 captured the wave-packet evolution and the spatial propagation dynamics of the electron Airy beam.

5 Trajectories measurement and error analysis–

One of the challenges in this work is to calibrate the effective distance that the beam travels from the focal plane. We image different planes of propagation by decreasing the focal length of the magnetic lens. In order to calibrate the propagation (z) axis we made the following analysis: We measured the Bragg diffraction patterns from the periodic reference grating (BR) with $\Lambda_{x_{BR}} = 100$ nm (for different setting of the magnetic lens). The linear trajectory of the first diffraction order as a function of z is given by[4]:

$$Peak_{x(BR)}(z) = \frac{\lambda_B}{\Lambda_{x_{BR}}} f + \frac{\lambda_B}{\Lambda_{x_{BR}}} z. \tag{11}$$

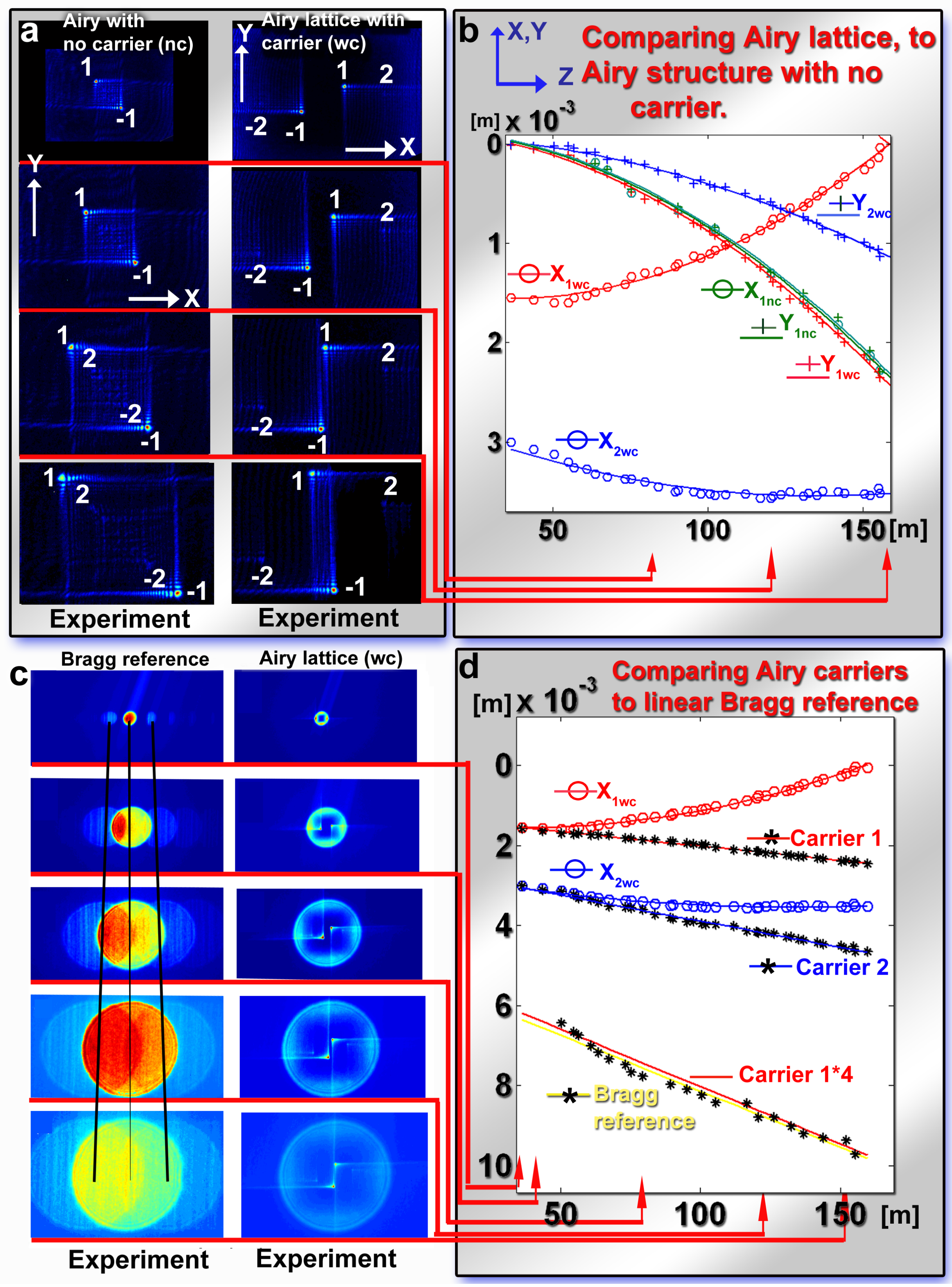

Figure 4 | **Calibrating the curved trajectories and comparing the diffractions of three structures. a, b,** Comparing Airy lattice to Airy structure with no carrier. The y deflection trajectory of Airy lattice (red) is equal to the x and y trajectories (green) of the Airy structure with no carrier as expected. **c, d** calibrating the carrier curves. The linear trajectory of Bragg structure is almost equal to 4 times the Airy carrier as expected.

where f is the focal length of the lens. The deflection of the first order was measured by the camera for each lens setting. As for the diffraction of the Airy wave through the mask with carrier (AWC) $\Lambda_{x_{BR}} = 400\ nm$, it has both quadratic and linear velocity components in x direction, i.e. the peak location of the strongest lobe is given by [5]:

$$Peak_{x(Ai)}(z) = \frac{\lambda_B}{\Lambda_{x_{Ai}}} f + \frac{\lambda_B}{\Lambda_{x_{Ai}}} z - \frac{1}{4k_B^2 x_0^3} z^2 \quad , \tag{12}$$

whereas in the Y direction we have only quadratic component, hence the peak location is:

$$Peak_{y(Ai)}(z) = \frac{1}{4k_B^2 x_0^3} z^2 \quad . \tag{13}$$

Therefore, the summation of y and x is:

$$Peak_{x(Ai)}(z) + Peak_{y(Ai)}(z) = \frac{\lambda_B}{\Lambda_{x_{Ai}}} f + \frac{\lambda_B}{\Lambda_{x_{Ai}}} z \quad , \tag{14}$$

which is also linearly increasing with a constant transverse velocity in z. This serves as the z axis of the measurement. Since the period here is $\Lambda_{x(Ai)} = 400$ nm, vs. only $\Lambda_{x(BR)} = 100$ nm for the Bragg reference mask, the carrier curve in the case of the Airy beam should be 4 times lower as verified experimentally. We can therefore verify the calibration by comparing the two measurements, as shown in Fig. 4c, d. We can also calibrate the quadratic components and compare the Airy lattice with carrier to Airy structure with no carrier shown in Fig. 4a, b: The Airy with no carrier (Anc) has no carrier modulation but was designed with the exact quadratic coefficients as the Airy lattice. The equations of motion from this structure are:

$$Peak_{y(Ai)}(z) = \frac{1}{4k_B^2 x_0^3} z^2 \quad . \tag{15}$$

$$Peak_{x(Ai)}(z) = \frac{1}{4k_B^2 x_0^3} z^2 \quad , \tag{16}$$

Here there is no carrier modulation, neither in x nor in y, hence the x and y trajectories starts from the center of axis and accelerates away from it (green lines in Fig. 4b). As expected trajectories nearly coincide with the results of the y axis of the Airy lattice (red curve) Fig. 4 a, b. We verified that the best fit to the curves is parabolic. The results are presented in Fig 5. As see the fitting parameters are better for the quadratic fit.

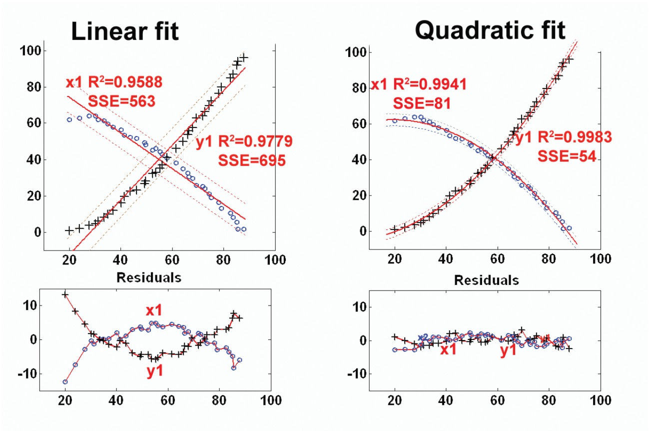

Figure 5 | Comparison between quadratic fit to the linear fit of the measured trajectories.

References

1. Berry, M. V. & Balazs, N. L. Nonspreading wave packets. *Am. J. Phys.* **47**, 264–267 (1979).
2. Siviloglou, G. A., Broky, J., Dogariu, A. & Christodoulides, D. N. Observation of accelerating Airy beams. *Phys. Rev. Lett.* **99**, 213901 (2007).
3. Verbeeck, J., Tian, H. & Schattschneider, P. Production and application of electron vortex beams. *Nature* **467**, 0028-0836 (2010).
4. McMorran, B. J., et al. Electron vortex beams with high quanta of orbital angular momentum. *Science* **14**, 192-195 (2011).
5. Siviloglou, G. A., Broky, J., Dogariu, A. & Christodoulides, D. N. Ballistic dynamics of Airy beams. *Opt. Lett.* **33**, 207–209 (2008).
6. Dai, H. T., Sun, X. W., Luo, D. & Liu, Y. J. Airy beams generated by a binary phase element made of polymer-dispersed liquid crystals. *Opt. Express* **17**, 19365 (2009).
7. Lee, W. H. Binary computer-generated holograms. *Appl. Opt.* **18**, 3661–3669 (1979).